PROCEEDINGS OF THE ROYAL SOCIETY A MATHEMATICAL, PHYSICAL & ENGINEERING SCIENCES

Thermal analysis of injectable, cellular-scale optoelectronics with pulsed power

Yuhang Li, Xiaoting Shi, Jizhou Song, Chaofeng Lü, Tae-il Kim, Jordan G. McCall, Michael R. Bruchas, John A. Rogers and Yonggang Huang

Proc. R. Soc. A 2013 **469**, 20130142, published 5 June 2013

PROCEEDINGS OF THE ROYAL SOCIETY A

rspa.royalsocietypublishing.org

Thermal analysis of injectable, cellular-scale optoelectronics with pulsed power

Yuhang Li[1,2,3,†], Xiaoting Shi[2,4,†], Jizhou Song[5], Chaofeng Lü[6], Tae-il Kim[7,8], Jordan G. McCall[9], Michael R. Bruchas[9], John A. Rogers[7] and Yonggang Huang[1,2]

[1]Department of Civil and Environmental Engineering, and [2]Department of Mechanical Engineering, Institute for Public Health and Medicine, Northwestern University, Evanston, IL 60208, USA

[3]Department of Engineering Mechanics, Zhejiang University, Hangzhou 310027, People's Republic of China

[4]Shanghai Key Laboratory of Materials Laser Processing and Modification, School of Materials Science and Engineering, Shanghai Jiaotong University, Shanghai 200240, People's Republic of China

[5]Department of Mechanical and Aerospace Engineering, University of Miami, Coral Gables, FL 33146, USA

[6]Department of Civil Engineering and Soft Matter Research Center, Zhejiang University, Hangzhou 310058, People's Republic of China

[7] Frederick Seitz Materials Research Laboratory, Department of Materials Science and Engineering, University of Illinois at Urbana-Champaign, Urbana, IL 61801, USA

[8]School of Chemical Engineering, Sungkyunkwan University (SKKU), Suwon 440-746, Korea

[9]Department of Anesthesiology, Division of Basic Research; Washington University Pain Center; Department of Anatomy and Neurobiology; Division of Biological and Biomedical Sciences, Washington University School of Medicine, St Louis, MO 63110, USA

An ability to insert electronic/optoelectronic systems into precise locations of biological tissues provides powerful capabilities, especially in neuroscience such as optogenetics where light can activate/deactivate critical cellular signalling and neural systems. In such cases, engineered thermal management is essential, to

Research

Cite this article: Li Y, Shi X, Song J, Lü C, Kim T, McCall JG, Bruchas MR, Rogers JA, Huang Y. 2013 Thermal analysis of injectable, cellular-scale optoelectronics with pulsed power. Proc R Soc A 469: 20130142. http://dx.doi.org/10.1098/rspa.2013.0142

Received: 27 February 2013
Accepted: 8 May 2013

Subject Areas:
mechanical engineering

Keywords:
thermal analysis, optoelectronics, light-emitting diode, scaling law

Authors for correspondence:
Jizhou Song
e-mail: jsong8@miami.edu
Yonggang Huang
e-mail: y-huang@northwestern.edu

[†]These authors contributed equally to this study.

Royal Society Publishing
Informing the science of the future

avoid adverse effects of heating on normal biological processes. Here, an analytic model of heat conduction is developed for microscale, inorganic light-emitting diodes (μ-ILEDs) in a pulsed operation in biological tissues. The analytic solutions agree well with both three-dimensional finite-element analysis and experiments. A simple scaling law for the maximum temperature increase is presented in terms of material (e.g. thermal diffusivity), geometric (e.g. μ-ILED size) and loading parameters (e.g. pulsed peak power, duty cycle and frequency). These results provide useful design guidelines not only for injectable μ-ILED systems, but also for other similar classes of electronic and optoelectronic components.

1. Introduction

Integration of electronic/optoelectronic systems with the human body can provide powerful diagnostic and therapeutic capabilities. Stretchable electronics opened new avenues for electronic circuits, light-emitting diodes (LEDs), sensors and other components with the ability to bend, twist and stretch, for wrapping the external surfaces of soft tissues (e.g. brain, skin and heart) [1–8]. A shortcoming of such device architectures is that they do not provide the ability to insert electronic/optoelectronic systems into precise locations of biological tissues. An example of a need for this type of functionality in neuroscience is in optogenetics, where localized delivery of light into the depth of the brain allows cell type selective control of cellular signalling and neural systems [9,10]. Strategies exploiting passive penetrating electrodes or optical fibres with interconnections to externally located electronics control/acquisition systems or light sources are valuable but suffer from challenges associated with tissue lesioning during insertion, persistent irritation that follows, and extreme engineering difficulties in thermal management [3,11,12]. Recently, Kim *et al.* [13] developed injectable, wireless devices that incorporate arrays of microscale, inorganic light-emitting diodes (μ-ILEDs) with lateral dimensions $100 \times 100\,\mu m^2$ and thicknesses of 6.45 μm (approx. 1000 times smaller than conventional LEDs with a dimension of approx. $1 \times 1 \times 0.1\,mm^3$), delivered into the tissue using a releasable microneedle. The resulting technology allows precise and patterned delivery of light directly to cellular-scale sub-regions in the depth of the brain. The injection of these devices into the mouse brain enables completely wireless and programmed behaviour control over freely moving animals. Figure 1*a* schematically shows the cross section of four μ-ILEDs coated with a thin (6 μm) layer of benzocyclobutene (BCB) on a 18 μm thick polyethylene terephthalate (PET) substrate in an explanted piece of tissue from the brain of a mouse with 9 mm length, 4 mm width and 4 mm thickness held at $T_\infty = 37^\circ C$ by a thermal stage. The thickness of tissue above the μ-ILEDs is denoted by h_0 and that below by h_1.

The thermal characteristics of these μ-ILEDs in the tissue are critically important because excessive heating (even 1–2°C temperature increase) may cause tissue lesioning and adverse reaction [14]. By operating μ-ILEDs in low duty cycle, pulsed modes, commonly used to mimic physiologically relevant firing pattern [15], difficulties in thermal management are significantly reduced. Under pulsed power (or current) as shown in figure 1*b*, the temperature of μ-ILED first increases and then reaches saturation at a stable level with maximum temperature that depends on material (e.g. thermal conductivity), geometric (e.g. μ-ILED size) and loading parameters (e.g. pulsed peak power, duty cycle and frequency) [16]. For better understanding of the device operation and establishing design guidelines for μ-ILED configurations that minimize thermal effects, an analytic model for pulsed mode operation is developed in this paper. The analytic model is validated by finite-element analysis (FEA) and experiments. The maximum temperature of μ-ILED is obtained analytically, and a simple scaling law for the maximum temperature change is established to enable optimized device performance. Section 2 gives the thermal analysis for a single μ-ILED in the tissue, while §3 presents the results for four μ-ILEDs as in experiments, and comparison with experiments.

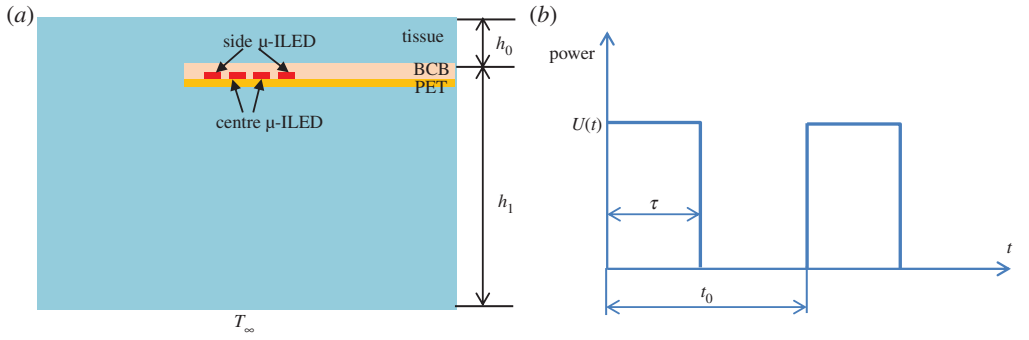

Figure 1. (*a*) Cross-sectional illustration of μ-ILEDs in biological tissue, (*b*) a unit pulsed power applied to the μ-ILEDs. (Online version in colour.)

2. Thermal analysis for a single inorganic light-emitting diode in the tissue

In the device of Kim *et al.* [13], four μ-ILEDs coated with a 6 μm thick layer of a polymer (BCB) on a 18 μm thick sheet of PET substrate are left in the mouse tissue after removing the injection microneedle (figure 1*a*). A pulsed power is applied to the μ-ILEDs to deliver light to cellular-scale sub-regions to control the animal behaviour. The temperature increase for the system of a single μ-ILED in the tissue is determined in this section, which then gives the temperature increase for a μ-ILED array by the method of superposition in §3.

The in-plane size $L \times L$ (approx. $100 \times 100\,\mu m$) of μ-ILED is much larger than its thickness h_{LED} (approx. 6.45 μm) such that heat transfer mainly occurs through the top and bottom surfaces of μ-ILED. For simplicity, an axisymmetric model is adopted to obtain the analytical solution, which is validated by the three-dimensional FEA in this section. The μ-ILED can then be modelled as a circular planar heat source. Its radius r_0 is determined by equating the surface area ($2\pi r_0^2$) to that of μ-ILED ($2L^2 + 4Lh_{LED}$), which gives $r_0 = \sqrt{L(L + 2h_{LED})/\pi}$. The effects of BCB and PET on the temperature distribution can be neglected because their thicknesses (approx. 10 μm) are much smaller than that of the tissue (approx. 4 mm), and their thermal properties (thermal conductivity approx. $0.3\,W m^{-1} K^{-1}$ and thermal diffusivity approx. $1.31 \times 10^{-7}\,m^2\,s^{-1}$) [17,18] are similar to those of tissue (thermal conductivity $0.6\,W m^{-1} K^{-1}$ and thermal diffusivity $1.58 \times 10^{-7}\,m^2\,s^{-1}$) [19,20].

Figure 2 shows a schematic of the analytic model for a single μ-ILED in the tissue. The heat source $Q(t) = Q_0 U(t)$ is applied to the μ-ILED, where Q_0 is the peak power and $U(t)$ is a unit pulsed power as shown in figure 1*b*. The duty cycle is defined as $D = \tau/t_0$ with τ as the pulse duration and t_0 as the period of the pulse. The cylindrical coordinate system (r, z) is established with the origin at the centre of the heat source and z-direction pointing downward. Let T_∞ denote the ambient temperature. The temperature change in the tissue from the ambient temperature, $\Delta T = T(r, z, t) - T_\infty$, satisfies

$$\frac{\partial \Delta T}{\partial t} - \alpha \left(\frac{\partial^2 \Delta T}{\partial r^2} + \frac{1}{r}\frac{\partial \Delta T}{\partial r} + \frac{\partial^2 \Delta T}{\partial z^2} \right) = 0, \tag{2.1}$$

where $\alpha = k/(c\rho)$ is thermal diffusivity of the tissue with k as thermal conductivity, c as specific heat capacity and ρ as mass density, respectively. The boundary conditions include zero heat flux at the top surface $-k\partial \Delta T/\partial z|_{z=-h_0} = 0$ since the natural convection is negligible [21,22], and constant temperature at the bottom surface $\Delta T|_{z=h_1} = 0$ since the tissue sits on a thermal stage. The temperature is continuous across the interface ($z = 0$) where the heat source is located, i.e. $\Delta T|_{z=0^+} = \Delta T|_{z=0^-}$, and the heat generation requires $-k\partial \Delta T/\partial z|_{z=0^+} + k\partial \Delta T/\partial z|_{z=0^-} = 0$ for $r > r_0$ and $-k(\partial \Delta T/\partial z)|_{z=0^+} + k(\partial \Delta T/\partial z)|_{z=0^-} = Q(t)/(\pi r_0^2)$ for $0 \le r \le r_0$, where $Q(t)/(\pi r_0^2)$ is the area density of the heat source.

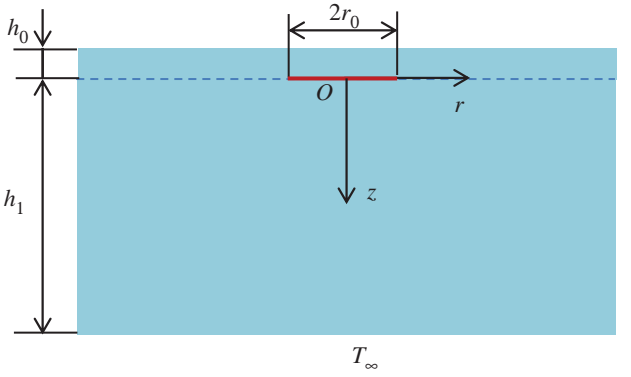

Figure 2. Schematic of the analytically modelled system with one single μ-ILED in biological tissue. (Online version in colour.)

The pulsed power $Q(t)$ can be expressed in Fourier series as

$$Q(t) = Q_0 \begin{cases} 1 & 0 < t \le \tau \\ 0 & \tau < t \le t_0 \end{cases} = Q_0 \left(a_0 + \sum_{n=1}^{\infty} a_n \cos n\omega t + \sum_{n=1}^{\infty} b_n \sin n\omega t \right), \tag{2.2}$$

where $\omega = 2\pi/t_0$, $a_0 = D = \tau/t_0$, $a_n = \sin(2n\pi D)/(n\pi)$ and $b_n = [1 - \cos(2n\pi D)]/(n\pi)$. We first obtain the temperature increase due to a sinusoidal power in equation (2.2) and then use method of superposition to find the temperature increase due to the pulsed power.

For a sinusoidal power $Q_0 \cos(\omega t)$ [or $Q_0 \sin(\omega t)$], which can be written as the real (or imaginary) part of $Q_0 e^{i\omega t}$, the temperature increase will have the same frequency such that it can be expressed as $\theta(r, z; \omega) e^{i\omega t}$. Substitution of $\theta(r, z; \omega) e^{i\omega t}$ into equation (2.1) yields

$$\frac{\partial^2 \theta}{\partial r^2} + \frac{1}{r}\frac{\partial \theta}{\partial r} + \frac{\partial^2 \theta}{\partial z^2} - i\frac{\omega}{\alpha}\theta = 0, \tag{2.3}$$

which can be solved via Hankel transform $\bar{\theta}(s, z; \omega) = \int_0^\infty \theta(r, z; \omega) J_0(sr) r dr$, where J_0 is the 0th-order Bessel function of the first kind [23]. The Hankel transform of equation (2.3) gives

$$\frac{d^2 \bar{\theta}}{dz^2} - \left(s^2 + i\frac{\omega}{\alpha} \right) \bar{\theta} = 0, \tag{2.4}$$

which has a solution

$$\bar{\theta} = A(s) e^{z\sqrt{s^2 + i(\omega/\alpha)}} + B(s) e^{-z\sqrt{s^2 + i(\omega/\alpha)}}, \tag{2.5}$$

where $A(s)$ and $B(s)$ are coefficients to be determined by boundary conditions and are denoted by A_0 and B_0 for the tissue above the μ-ILED and A_1 and B_1 for that below the μ-ILED. The Hankel transform of boundary conditions and continuity conditions after equation (2.1) gives these coefficients as

$$\begin{Bmatrix} A_0 \\ B_0 \\ A_1 \\ B_1 \end{Bmatrix} = \frac{Q_0}{2\pi r_0 k} \frac{J_1(sr_0) e^{(h_1 + h_0)\sqrt{s^2 + i(\omega/\alpha)}}}{s\sqrt{s^2 + i(\omega/\alpha)} \cosh[(h_1 + h_0)\sqrt{s^2 + i(\omega/\alpha)}]}$$
$$\times \begin{Bmatrix} e^{h_0\sqrt{s^2 + i(\omega/\alpha)}} \sinh\left(h_1 \sqrt{s^2 + i(\omega/\alpha)} \right) \\ e^{-h_0\sqrt{s^2 + i(\omega/\alpha)}} \sinh\left(h_1 \sqrt{s^2 + i(\omega/\alpha)} \right) \\ -e^{-h_1\sqrt{s^2 + i(\omega/\alpha)}} \cosh\left(h_0 \sqrt{s^2 + i(\omega/\alpha)} \right) \\ e^{h_1\sqrt{s^2 + i(\omega/\alpha)}} \cosh\left(h_0 \sqrt{s^2 + i(\omega/\alpha)} \right) \end{Bmatrix}, \tag{2.6}$$

where J_1 is the 1st-order Bessel function of the first kind [23]. The inverse Hankel transform $\theta(r,z;\omega)=\int_0^\infty \bar{\theta}(s,z;\omega)J_0(sr)s\,\mathrm{d}s$ gives the temperature increase in the tissue above and below the μ-ILED as

$$\theta(r,z;\omega)=\begin{cases}\dfrac{Q_0}{\pi r_0 k}\displaystyle\int_0^\infty J_1(sr_0)J_0(sr)\frac{\sinh\left(h_1\sqrt{s^2+\mathrm{i}(\omega/\alpha)}\right)\cosh\left[(h_0+z)\sqrt{s^2+\mathrm{i}(\omega/\alpha)}\right]}{\sqrt{s^2+\mathrm{i}(\omega/\alpha)}\cosh\left[(h_1+h_0)\sqrt{s^2+\mathrm{i}(\omega/\alpha)}\right]}\mathrm{d}s & -h_0\le z\le 0\\ \dfrac{Q_0}{\pi r_0 k}\displaystyle\int_0^\infty J_1(sr_0)J_0(sr)\frac{\cosh\left(h_0\sqrt{s^2+\mathrm{i}(\omega/\alpha)}\right)\sinh\left[(h_1-z)\sqrt{s^2+\mathrm{i}(\omega/\alpha)}\right]}{\sqrt{s^2+\mathrm{i}(\omega/\alpha)}\cosh\left[(h_1+h_0)\sqrt{s^2+\mathrm{i}(\omega/\alpha)}\right]}\mathrm{d}s & 0<z\le h_1.\end{cases} \tag{2.7}$$

It should be noted that the maximum temperature increase in the system occurs in μ-ILED. The temperature increase in the μ-ILED is quite uniform due to its large thermal conductivity (approx. $160\,\mathrm{W\,m^{-1}\,K^{-1}}$) when compared with that of the tissue (approx. $0.6\,\mathrm{W\,m^{-1}\,K^{-1}}$). It can be well approximately by the average temperature of the μ-ILED over the entire region of μ-ILED ($z=0$, $0\le r\le r_0$) [21,22], which gives

$$\theta_{\mathrm{LED}}(\omega)=\frac{2Q_0}{\pi r_0 k}\int_0^\infty \frac{J_1^2(\xi)}{\xi}\frac{\sinh\left((h_1/r_0)\sqrt{\xi^2+\mathrm{i}(\omega/\alpha)r_0^2}\right)\cosh\left((h_0/r_0)\sqrt{\xi^2+\mathrm{i}(\omega/\alpha)r_0^2}\right)}{\sqrt{\xi^2+\mathrm{i}(\omega/\alpha)r_0^2}\cosh\left(((h_1+h_0)/r_0)\sqrt{\xi^2+\mathrm{i}(\omega/\alpha)r_0^2}\right)}\mathrm{d}\xi. \tag{2.8}$$

The temperature increase in μ-ILED due to a pulsed power is then obtained by

$$\Delta T_{\mathrm{LED}}(t;\omega)=D\theta_{\mathrm{LED}}(0)+\sum_{n=1}^{\infty}|\theta_{\mathrm{LED}}(n\omega)|\left[\begin{array}{l}\dfrac{\sin(2n\pi D)}{n\pi}\cos(n\omega t+\gamma_n)\\ +\dfrac{1-\cos(2n\pi D)}{n\pi}\sin(n\omega t+\gamma_n)\end{array}\right], \tag{2.9}$$

where γ_n is the phase angle of $\theta_{\mathrm{LED}}(n\omega)$.

The size of μ-ILED is usually approximately 100 μm, while the thickness h_0 and h_1 are approximately 1 mm. For such large ratios of h_0/r_0 and h_1/r_0, equation (2.8) can be approximated to

$$\frac{\theta_{\mathrm{LED}}}{Q_0/(k\sqrt{A})}\approx\sqrt{\frac{2}{\pi}}\int_0^\infty\frac{J_1^2(\xi)}{\xi\sqrt{\xi^2+\mathrm{i}\beta}}\mathrm{d}\xi=\sqrt{\frac{2}{\pi}}\frac{\sqrt{\mathrm{i}\beta}-J_1(2\sqrt{\mathrm{i}\beta})+L_1(2\sqrt{\mathrm{i}\beta})}{2\mathrm{i}\beta}, \tag{2.10}$$

where $\beta=A/A(\alpha t_0)$, $A\,(=2\pi r_0^2)$ is the total surface area of μ-ILED and is given by $A=2L^2+4Lh_{\mathrm{LED}}$ for a square μ-ILED of size L and thickness h_{LED}, and L_1 is the 1st-order modified Struve function [23]. The normalized temperature increase, given by the left-hand side of equation (2.10), depends only on a single non-dimensional parameter β. Equation (2.9) can then be simplified to

$$\frac{\Delta T_{\mathrm{LED}}(t)}{Q_0/(k\sqrt{A})}\approx\sqrt{\frac{32}{9\pi^3}}D+\sqrt{\frac{2}{\pi}}\sum_{n=1}^{\infty}\left\{\left|\frac{\sqrt{\mathrm{i}n\beta}-J_1(2\sqrt{\mathrm{i}n\beta})+L_1(2\sqrt{\mathrm{i}n\beta})}{2\mathrm{i}n\beta}\right|*\left[\frac{\sin(2n\pi D)}{n\pi}\cos\left(\frac{2\pi nt}{t_0}+\delta_n\right)+\frac{1-\cos(2n\pi D)}{n\pi}\sin\left(\frac{2\pi nt}{t_0}+\delta_n\right)\right]\right\}, \tag{2.11}$$

where δ_n is the phase angle of $\left\{\sqrt{\mathrm{i}n\beta}-J_1\left(2\sqrt{\mathrm{i}n\beta}\right)+L_1\left(2\sqrt{\mathrm{i}n\beta}\right)\right\}/(2\mathrm{i}n\beta)$. The maximum normalized temperature increase (with respect to time) in μ-ILED then depends only on D and β, i.e. a simple scaling law

$$\Delta T_{\mathrm{LED}}^{\max}\approx\frac{Q_0}{k\sqrt{A}}\bar{T}(D,\beta), \tag{2.12}$$

where $\bar{T}$ is a non-dimensional function and is shown versus the duty cycle D in figure 3 for $\beta=0.048$, 0.48 and 4.8, where $\beta=0.48$ corresponds to the parameters in the experiment

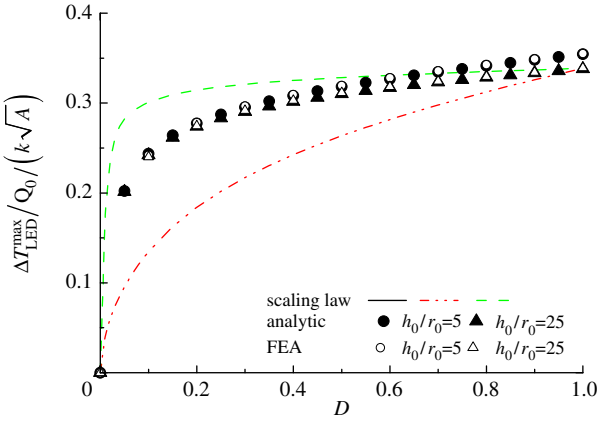

Figure 3. Maximum normalized μ-ILED temperature increase by analytic, scaling law and FEA versus duty cycle. (Online version in colour.)

($k = 0.6\,\mathrm{W\,(m\cdot K)^{-1}}$, $c = 4121\,\mathrm{J(kg\cdot K)^{-1}}$, $\rho = 1040\,\mathrm{kg\,m^{-3}}$, $L = 100\,\mu\mathrm{m}$, $h_{\mathrm{LED}} = 6.45\,\mu\mathrm{m}$ and $t_0 = 0.33\,\mathrm{s}$) [13,20]. Equation (2.12) and figure 3 clearly suggest that small peak power Q_0, duty cycle D, period t_0, and large surface area A of μ-ILED are effective to reduce the maximum temperature increase. The thermal properties of the tissue play a mixed role; large thermal conductivity k and small thermal diffusivity α also reduce the maximum temperature increase. Such a scaling law is useful to provide design guidelines to minimize the thermal effect of the μ-ILED.

Unlike the scaling law in equation (2.12) that depends on D and β, the maximum normalized temperature increase obtained from the analytic solution in equation (2.9) also depends on h_0/r_0 and h_1/r_0. It is shown in figure 3 for $\beta = 0.48$ and $(h_0 + h_1)/r_0 = 67$ as in the experiment [13] and two very different ratios $h_0/r_0 = 5$ (solid circles) and 25 (solid triangles), which all agree well with the scaling law in equation (2.12). Three-dimensional FEA is also used to validate the analytic solution. The continuum element DC3D8 in the ABAQUS software [24] is adopted to model the three-dimensional geometries of μ-ILED ($100 \times 100 \times 6.45\,\mu\mathrm{m}$), BCB ($8\,\mathrm{mm} \times 100\,\mu\mathrm{m} \times 6\,\mu\mathrm{m}$) and PET ($8\,\mathrm{mm} \times 500\,\mu\mathrm{m} \times 18\,\mu\mathrm{m}$). The thermal conductivity, heat capacity and mass density are $160\,\mathrm{W(m\cdot K)^{-1}}$, $700\,\mathrm{J(kg\cdot K)^{-1}}$ and $2329\,\mathrm{kg\,m^{-3}}$ for μ-ILED [25], $0.3\,\mathrm{W(m\cdot K)^{-1}}$, $1050\,\mathrm{J(kg\cdot K)^{-1}}$ and $2180\,\mathrm{kg\,m^{-3}}$ for BCB [17], $0.24\,\mathrm{W(m\cdot K)^{-1}}$, $1370\,\mathrm{J(kg\cdot K)^{-1}}$ and $1000\,\mathrm{kg\,m^{-3}}$ for PET [18]. The tissue is 4mm thick and has the in-plane dimension $9 \times 4\,\mathrm{mm}$. As shown in figure 3, results from three-dimensional FEA agree well with the analytic solution.

3. Thermal analysis for inorganic light-emitting diode arrays in the tissue

The results in §2 for one single μ-ILED in the tissue form the basis for studying the μ-ILED arrays in the tissue. An array with four μ-ILEDs, shown in figure 4, is used to illustrate the approach. The distance between the centres of two adjacent μ-ILEDs is denoted by r_{d}. With the origin at the centre of arrays (figure 4), the coordinates of μ-ILED centres are $(\pm 3r_{\mathrm{d}}/2, 0)$ and $(\pm r_{\mathrm{d}}/2, 0)$. The temperature increase at any location in the tissue can be obtained from the result of one single μ-ILED in §2 by the method of superposition. For example, the temperature increase at the centre point P_1 of the top surface due to a sinusoidal power $Q_0\cos(\omega t)$ [or $Q_0\sin(\omega t)$] per μ-ILED is obtained from equation (2.7) as $\theta_{\mathrm{surface}}(\omega) = 2\theta(r = r_{\mathrm{d}}/2, z = -h_0; \omega) + 2\theta(r = 3r_{\mathrm{d}}/2, z = -h_0; \omega)$, i.e.

$$\theta_{\mathrm{surface}}(\omega) = \frac{2Q_0}{\pi r_0 k}\int_0^\infty J_1(\xi)\left[J_0\left(\frac{r_{\mathrm{d}}\xi}{2r_0}\right) + J_0\left(\frac{3r_{\mathrm{d}}\xi}{2r_0}\right)\right] \times \frac{\sinh\left((h_1/r_0)\sqrt{\xi^2 + \mathrm{i}(\omega/\alpha)r_0^2}\right)}{\sqrt{\xi^2 + \mathrm{i}(\omega/\alpha)r_0^2}\cosh(((h_1 + h_0)/r_0)\sqrt{\xi^2 + \mathrm{i}(\omega/\alpha)r_0^2})}\mathrm{d}\xi. \tag{3.1}$$

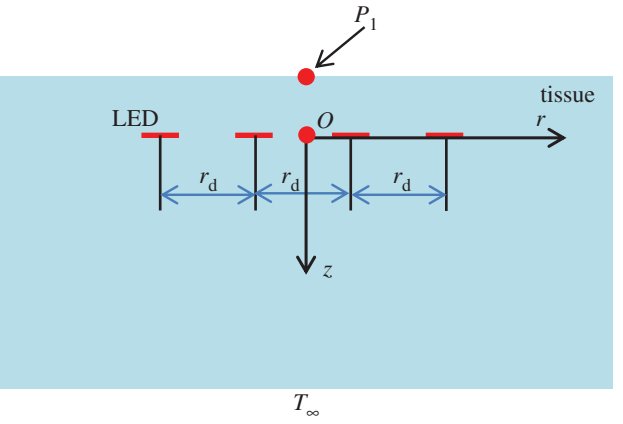

Figure 4. Schematic of the analytically modelled system with four μ-ILEDs in the tissue. (Online version in colour.)

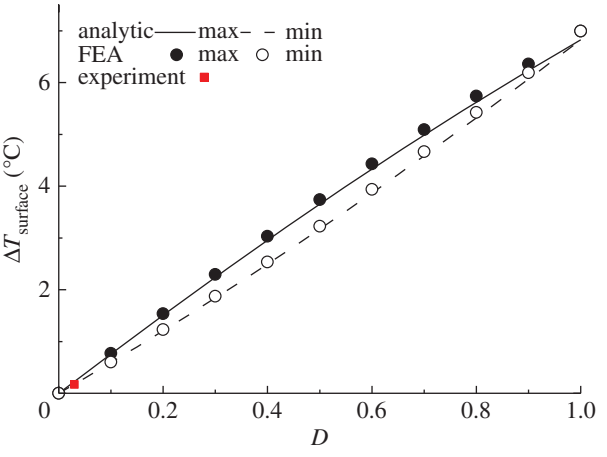

Figure 5. Surface temperature increase determined by analytic model, FEA and experiment versus duty cycle. (Online version in colour.)

The temperature increase at the centre point P_1 of the top surface due to the pulsed power is then obtained as

$$\Delta T_{\text{surface}}(t;\omega) = D\theta_{\text{surface}}(0) + \sum_{n=1}^{\infty} |\theta_{\text{surface}}(n\omega)| \left[\begin{array}{l} \dfrac{\sin(2n\pi D)}{n\pi} \cos(n\omega t + \zeta_n) \\ + \dfrac{1-\cos(2n\pi D)}{n\pi} \sin(n\omega t + \zeta_n) \end{array} \right], \tag{3.2}$$

where ζ_n is the phase angle of $\theta_{\text{surface}}(n\omega)$ and Q_0 is the peak power per μ-ILED. Figure 5 shows the maximum and minimum temperature increase versus the duty cycle for the frequency 3 Hz, peak power $Q_0 = 2.5$ mW, $r_0 = 60\,\mu$m, $r_d = 200\,\mu$m, $h_0 = 0.3$ mm and $h_1 = 3.7$ mm. These results agree very well with those obtained from three-dimensional FEA, also shown in figure 3. For the duty cycle 3 per cent, the experimentally measured temperature increase is 0.17°C [13], which is indeed between the maximum and minimum temperature increase 0.22°C and 0.17°C given by the analytic model, as is shown in figure 5.

For a sinusoidal power $Q_0 \cos(\omega t)$ [or $Q_0 \sin(\omega t)$], the maximum temperature increase of the centre μ-ILED can also be obtained from equations (2.7) and (2.8) by the method of superposition

as $\theta_{\text{centre LED}}(\omega) = \theta_{\text{LED}}(\omega) + 2\theta(r = r_{\text{d}}, z = 0; \omega) + \theta(r = 2r_{\text{d}}, z = 0; \omega)$, which gives

$$\theta_{\text{centre LED}}(\omega) = \frac{2Q_0}{\pi r_0 k} \int_0^\infty \left\{ \frac{J_1(\xi)\left[\frac{J_1(\xi)}{\xi} + J_0\left(\frac{r_{\text{d}}}{r_0}\xi\right) + \frac{1}{2}J_0\left(\frac{2r_{\text{d}}}{r_0}\xi\right)\right] * \sinh\left(\frac{h_1}{r_0}\sqrt{\xi^2 + \mathrm{i}\frac{\omega}{\alpha}r_0^2}\right)\cosh\left(\frac{h_0}{r_0}\sqrt{\xi^2 + \mathrm{i}\frac{\omega}{\alpha}r_0^2}\right)}{\sqrt{\xi^2 + \mathrm{i}\frac{\omega}{\alpha}r_0^2}\cosh\left(\frac{h_0+h_1}{r_0}\sqrt{\xi^2 + \mathrm{i}\frac{\omega}{\alpha}r_0^2}\right)} \right\} \mathrm{d}\xi. \tag{3.3}$$

For large ratios of h_0/r_0 and h_1/r_0 as in experiments [13], the above equation is simplified to

$$\frac{\theta_{\text{centre LED}}}{Q_0/(k\sqrt{A})} = \sqrt{\frac{2}{\pi}} \int_0^\infty \frac{J_1(\xi)}{\sqrt{\xi^2 + \mathrm{i}\beta}} \left[\frac{J_1(\xi)}{\xi} + J_0\left(\frac{\sqrt{2\pi}r_{\text{d}}}{\sqrt{A}}\xi\right) + \frac{1}{2}J_0\left(\frac{2\sqrt{2\pi}r_{\text{d}}}{\sqrt{A}}\xi\right)\right] \mathrm{d}\xi, \tag{3.4}$$

which shows the normalized temperature increase $\theta_{\text{centre LED}}/[Q_0/(k\sqrt{A})]$ depends only on two non-dimensional parameters: $r_{\text{d}}/\sqrt{A}$ and β.

The normalized temperature increase can then be obtained by

$$\begin{aligned}
&\frac{\Delta T_{\text{centre LED}}(t)}{Q_0/(k\sqrt{A})} \\
&= \sqrt{\frac{2}{\pi^3}} D\left[\frac{4}{3} + 2E\left(\sqrt{2\pi}\frac{r_{\text{d}}}{\sqrt{A}}\right) + E\left(2\sqrt{2\pi}\frac{r_{\text{d}}}{\sqrt{A}}\right)\right] \\
&\quad + \sqrt{\frac{2}{\pi}} \sum_{n=1}^{\infty} \left\{ \left| \int_0^\infty \frac{J_1(\xi)}{\sqrt{\xi^2 + \mathrm{i}\cdot\mathrm{n}\beta}} \left[\frac{J_1(\xi)}{\xi} + J_0\left(\frac{\sqrt{2\pi}r_{\text{d}}}{\sqrt{A}}\xi\right) + \frac{1}{2}J_0\left(\frac{2\sqrt{2\pi}r_{\text{d}}}{\sqrt{A}}\xi\right)\right] \mathrm{d}\xi \right| * \right. \\
&\quad \left. \left[\frac{\sin(2n\pi D)}{n\pi}\cos\left(\frac{2\pi nt}{t_0} + \eta_n\right) + \frac{1 - \cos(2n\pi D)}{n\pi}\sin\left(\frac{2\pi nt}{t_0} + \eta_n\right)\right] \right\},
\end{aligned} \tag{3.5}$$

where E is complete elliptic integral of the second kind [13], and η_n is the phase angle of

$$\int_0^\infty \frac{J_1(\xi)}{\sqrt{\xi^2 + \mathrm{i}\cdot\mathrm{n}\beta}} \left[\frac{J_1(\xi)}{\xi} + J_0\left(\frac{\sqrt{2\pi}r_{\text{d}}}{\sqrt{A}}\xi\right) + \frac{1}{2}J_0\left(\frac{2\sqrt{2\pi}r_{\text{d}}}{\sqrt{A}}\xi\right)\right] \mathrm{d}\xi.$$

The above equation shows that the maximum normalized temperature increase $\Delta T^{\max}_{\text{centre LED}}/[Q_0/(k\sqrt{A})]$ depends on $r_{\text{d}}/\sqrt{A}$, β and D. Figure 6 shows the maximum normalized temperature increase of the centre μ-ILED versus the normalized non-dimensional parameter β with duty cycle $D = 10\%$ and 50%, and $r_{\text{d}}/\sqrt{A} = 1.3, 3.3$ and 5.3. The maximum normalized temperature increase of centre μ-ILED drops significantly within the range of β from 0 to 40 and then remains almost unchanged for $\beta > 40$. The results suggest that large $r_{\text{d}}/\sqrt{A}$, small β and D reduce the maximum temperature increase.

It should be noted that the above analytic model is applicable to both dead tissue on a thermal stage and living tissue, though the latter involves heat loss due to blood flow (in the living tissue) [13]. This effect can be accounted for by adopting an effective fraction of heat loss, which is determined from experiments at one pulse frequency. Based on this effective fraction, the temperature at other frequencies or duty cycles agree well with experiments (error < 5%) [13].

We also studied the effect of thermal contact resistance on the μ-ILED temperature using FEA. For the thermal contact resistance on the typical order of $10^{-6}\,\mathrm{m}^2 \cdot \mathrm{KW}^{-1}$ [26], it is shown the μ-ILED temperature increase under power 10 mW and duty cycle 100 per cent (for a single μ-ILED in the tissue) increases 4.9 per cent from 4.45°C to 4.67°C such that the thermal resistance is negligible.

4. Conclusions

An analytic model, validated by FEA and experiments, is established to study the thermal behaviour of μ-ILEDs operating in a pulsed mode in biological tissue. A simple scaling law for the temperature increase in a single μ-ILED shows that the maximum normalized temperature

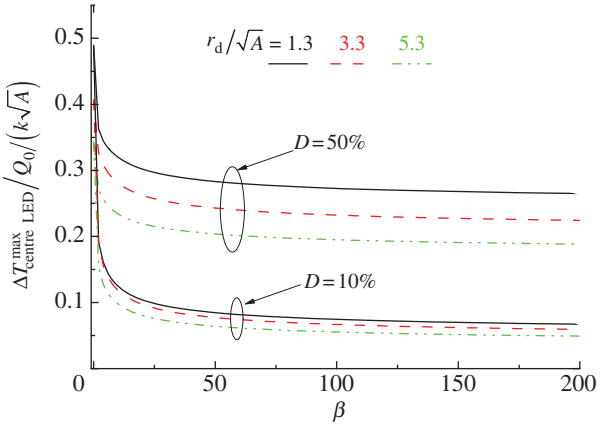

Figure 6. Maximum normalized temperature increase of centre μ-ILED versus normalized parameter β. (Online version in colour.)

increase depends only on two normalized parameters: duty cycle D and $\beta = A/(\alpha t_0)$, where A is the total surface area of μ-ILED, α is the thermal diffusivity of tissue and t_0 is the period of pulse power. Small peak power, duty cycle, period, thermal diffusivity of the tissue and large surface area of μ-ILED are effective in reducing the maximum temperature increase. The scaling law for the maximum temperature increase of the system of 4 μ-ILEDs in the tissue is also obtained by the method of superposition. In addition to D and β, the maximum temperature increase also depends on the normalized distance between two adjacent μ-ILEDs $r_d/\sqrt{A}$. Small D and β and large $r_d/\sqrt{A}$ are effective to reduce the maximum temperature increase. The analytic model can be extended to study other μ-ILEDs in the tissue with different layouts and materials, to provide design guidelines for avoiding adverse effects of heating.

J.S. acknowledges the support from the Provost Award from the University of Miami. C.L. acknowledges the support from the NSFC (grant no. 11172263) and the ZJNSF (grant no. R13A020001). Y.H. acknowledges the supports from NSF and NSFC. Supported by the NIH Common Fund; National Institute of Neurological Disorders and Stroke, NIH, R01NS081707 (MRB, JAR).

References

1. Kim DH *et al.* 2010 Dissolvable films of silk fibroin for ultrathin conformal bio-integrated electronics. *Nat. Mater.* **9**, 511–517. (doi:10.1038/NMAT2745)
2. Viventi J *et al.* 2010 A conformal, bio-interfaced class of silicon electronics for mapping cardiac electrophysiology. *Sci. Transl. Med.* **2**, 24ra22. (doi:10.1126/scitranslmed.3000738)
3. Tian B, Tzahi CK, Qing Q, Duan X, Xie P, Lieber CM. 2010 Three-dimensional, flexible nanoscale field effect transistors as localized bioprobes. *Science* **329**, 830–834. (doi:10.1126/science.1192033)
4. Kim DH *et al.* 2011 Epidermal electronics. *Science* **333**, 838–843. (doi:10.1126/science.1206157)
5. Qing Q, Pal SK, Tian B, Duan X, Timko BP, Tzahi CK, Murthy VN, Lieber CM. 2010 Nanowire transistor arrays for mapping neural circuits in acute brain slices. *Proc. Natl Acad. Sci. USA* **107**, 1882–1887. (doi:10.1073/pnas.0914737107)
6. Sekitani T, Someya T. 2012 Stretchable organic integrated circuits for large-area electronic skin surfaces. *MRS Bull.* **37**, 236–245. (doi:10.1557/mrs.2012.42)
7. Ordonez J, Schuettler M, Boehler C, Boretius T, Stieglitz T. 2012 Thin films and microelectrode arrays for neuroprosthetics. *MRS Bull.* **37**, 590–598. (doi:10.1557/mrs.2012.117)
8. Sekitani T, Yokota T, Zschieschang U, Klauk H, Bauer S, Takeuchi K, Takamiya M, Sakurai T, Someya T. 2009 Organic nonvolatile memory transistors for flexible sensor arrays. *Science* **326**, 1516–1519. (doi:10.1126/science.1179963)

9. Szobota S, Isacoff EY. 2010 Optical control of neuronal activity. *Annu. Rev. Biophys.* **39**, 329–348. (doi:10.1146/annurev.biophys.093008.131400)
10. Miesenböck G. 2011 Optogenetic control of cells and circuits. *Annu. Rev. Cell Dev. Biol.* **27**, 731–758. (doi:10.1146/annurev-cellbio-100109-104051)
11. Cao H, Gu L, Mohanty SK, Chiao JC. 2013 An integrated μLED optrode for optogenetic stimulation and electrical recording. *IEEE Trans. Biomed. Eng.* **60**, 225–229. (doi:10.1109/TBME.2012.2217395)
12. Tian B *et al.* 2012 Macroporous nanowire nanoelectronic scaffolds for synthetic tissues. *Nat. Mater.* **11**, 986–994. (doi:10.1038/nmat3404)
13. Kim TI *et al.* 2013 Injectable, cellular-scale optoelectronics with applications for wireless optogenetics. *Science* **340**, 211–216. (doi:10.1126/science.1232437)
14. Childs C. 2008 Human brain temperature: regulation, measurement and relationship with cerebral trauma: Part I. *Brit. J. Neurosurg.* **22**, 486–496. (doi:10.1080/02688690802245541)
15. Nunemaker CS, Defazio RA, Geusz ME, Herzog ED, Pitts GR, Moenter SM. 2001 Long-term recordings of networks of immortalized GnRH neurons reveal episodic patterns of electrical activity. *J. Neurophysiol.* **86**, 86–93.
16. Yang L, Hu J, Shin MW. 2008 Dynamic thermal analysis of high-power LEDs at pulse conditions. *IEEE Electron Dev. Lett.* **29**, 863–866. (doi:10.1109/LED.2008.2000953)
17. Modafe A, Ghalichechian N, Powers M, Khbeis M, Ghodssi R. 2005 Embedded benzocyclobutene in silicon: an integrated fabrication process for electrical and thermal isolation in MEMS. *Microelectron. Eng.* **82**, 154–167. (doi:10.1016/j.mee.2005.07.005)
18. van der Vegt AK, Govaert LE. 2005 *Polymeren*. Delft, The Netherlands: VSSD.
19. Elwassif MM, Kong Q, Vazquez M, Bikson M. 2006 Bio-heat transfer model of deep brain stimulation-induced temperature changes. *J. Neural Eng.* **3**, 306–315. (doi:10.1088/1741-2560/3/4/008)
20. Haemmerich D, Schutt DJ, Santos ID, Webster JG, Mahvi DM. 2005 Measurement of temperature-dependent specific heat of biological tissues. *Physiol. Meas.* **26**, 59–67. (doi:10.1088/0967-3334/26/1/006)
21. Li Y, Shi Y, Song J, Lü C, Kim TI, Rogers JA, Huang Y. 2013 Thermal properties of microscale inorganic light-emitting diodes in a pulsed operation. *J. Appl. Phys.* **113**, 144505. (doi:10.1063/1.4800858)
22. Kim HS *et al.* 2011 Unusual strategies for using indium gallium nitride grown on silicon (111) for solid-state lighting. *Proc. Natl Acad. Sci. USA* **108**, 10 072–10 077. (doi:10.1073/pnas.1102650108)
23. Abramowitz M, Stegun IA. 1964 *Handbook of mathematical functions: with formulas, graphs, and mathematical tables*, ch. 9–12,17. New York, NY: Dover.
24. ABAQUS. 2009 *Analysis user's manual v.6.9*. Pawtucket, RI: Dassault Systèmes.
25. Li R *et al.* 2012 Thermo-mechanical modeling of laser-driven non-contact transfer printing: two-dimensional analysis. *Soft Matter.* **8**, 7122–7127. (doi:10.1039/c2sm25339a)
26. Zhang K, Yuen MMF, Wang N, Miao JY, Xiao DGW, Fan HB. 2006 Thermal interface material with aligned CNT and its application in HB-LED packaging. In *56th Electronic Components and Technology Conf., San Diego, CA*, vol. 1 and 2, pp. 177–182. New York, NY: IEEE. (doi:10.1109/ECTC.2006.1645644)

PROCEEDINGS OF THE ROYAL SOCIETY A

rspa.royalsocietypublishing.org

Thermal analysis of injectable, cellular-scale optoelectronics with pulsed power

Yuhang Li, Xiaoting Shi, Jizhou Song, Chaofeng Lü, Tae-il Kim, Jordan G. McCall, Michael R. Bruchas, John A. Rogers and Yonggang Huang

Proc. R. Soc. A **469**, 20130142 (8 August 2013; Published online 5 June 2013) (doi:10.1098/rspa.2013.0142)

Correction

Cite this article: Li Y, Shi X, Song J, Lü C, Kim T, McCall JG, Bruchas MR, Rogers JA, Huang Y. 2013 Thermal analysis of injectable, cellular-scale optoelectronics with pulsed power. Proc R Soc A 469: 20130398. http://dx.doi.org/10.1098/rspa.2013.0398

Figure 3 is currently published as

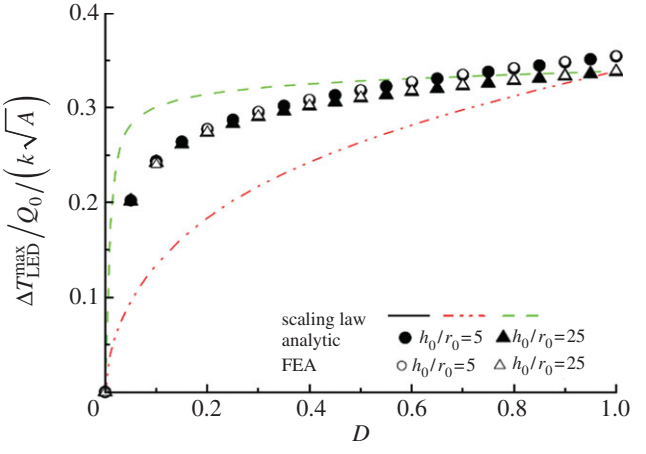

but it should read as shown below.

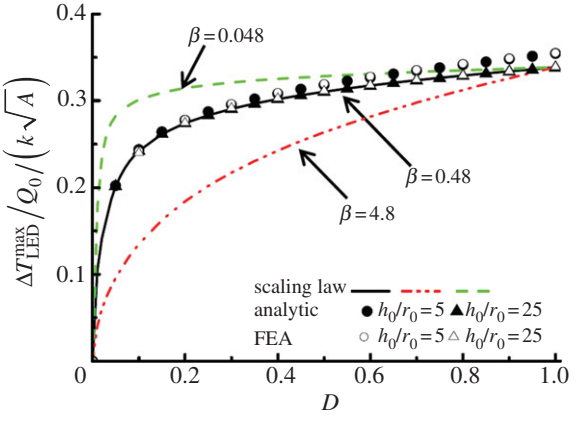

Royal Society Publishing
Informing the science of the future

The acknowledgements should have been published as follows:

J.S. acknowledges the support from the Provost Award from the University of Miami. C.L. acknowledges the support from the NSFC (grant no. 11172263) and the ZJNSF (grant no. R13A020001). Y.H. acknowledges support from NSF and NSFC. M.R.B. and J.A.R. acknowledge support from NIH Common Fund; National Institute of Neurological Disorders and Stroke (NIH R01NS081707).